Design Considerations of a Transverse Flux Machine for Direct-Drive Wind Turbine Applications

Preprint

Tausif Husain, Iftekhar Hasan, and Yilmaz Sozer
University of Akron

Iqbal Husain
North Carolina State University

Eduard Muljadi
National Renewable Energy Laboratory

Presented at the 2016 IEEE Energy Conversion Congress and Exposition
Milwaukee, Wisconsin
September 18–22, 2016

NREL is a national laboratory of the U.S. Department of Energy
Office of Energy Efficiency & Renewable Energy
Operated by the Alliance for Sustainable Energy, LLC

This report is available at no cost from the National Renewable Energy Laboratory (NREL) at www.nrel.gov/publications.

Conference Paper
NREL/CP-5D00-66391
January 2017

Contract No. DE-AC36-08GO28308

NOTICE

This report is available at no cost from the National Renewable Energy Laboratory (NREL) at www.nrel.gov/publications.

Available electronically at SciTech Connect http:/www.osti.gov/scitech

Available for a processing fee to U.S. Department of Energy and its contractors, in paper, from:

U.S. Department of Energy
Office of Scientific and Technical Information
P.O. Box 62
Oak Ridge, TN 37831-0062
OSTI http://www.osti.gov
Phone: 865.576.8401
Fax: 865.576.5728
Email: reports@osti.gov

Available for sale to the public, in paper, from:

U.S. Department of Commerce
National Technical Information Service
5301 Shawnee Road
Alexandria, VA 22312
NTIS http://www.ntis.gov
Phone: 800.553.6847 or 703.605.6000
Fax: 703.605.6900
Email: orders@ntis.gov

Cover Photos by Dennis Schroeder: (left to right) NREL 26173, NREL 18302, NREL 19758, NREL 29642, NREL 19795.

NREL prints on paper that contains recycled content.

Design Considerations of a Transverse Flux Machine for Direct-Drive Wind Turbine Applications

Tausif Husain[1] Iftekhar Hasan[1] Yilmaz Sozer[1] Iqbal Husain[2] Eduard Muljadi[3]

[1] ECE Department
The University of Akron
Akron, USA

[2] ECE Department
North Carolina State University
Raleigh, USA

[3] National Renewable Energy Laboratory
Golden, CO, USA

***Abstract*—This paper presents the design considerations of a double-sided transverse flux machine (TFM) for direct-drive wind turbine applications. The TFM has a modular structure with quasi-U stator cores and ring windings. The rotor is constructed with ferrite magnets in a flux-concentrating arrangement to achieve high air gap flux density. The design considerations for this TFM with respect to initial sizing, pole number selection, key design ratios, and pole shaping are presented in this paper. Pole number selection is critical in the design process of a TFM because it affects both the torque density and power factor under fixed magnetic and changing electrical loading. Several key design ratios are introduced to facilitate the design procedure. The effect of pole shaping on back-emf and inductance is also analyzed. These investigations provide guidance toward the required design of a TFM for direct-drive applications. The analyses are carried out using analytical and three-dimensional finite element analysis. A prototype is under construction for experimental verification.**

***Keywords*—review, transverse flux machine, permanent magnet machine, design consideration, pole number selection, pole shaping, design ratio, wind generator, high torque density.**

I. INTRODUCTION

Direct-drive configurations of electric machines in wind turbines avoid the drawbacks associated with gearing configurations. The concept of a transverse flux machine (TFM) was first introduced in 1885 by W. M. Morday. It gained more attention in the late 1980s after it was reintroduced and named as such by Weh [1]–[3]. The major advantage of a TFM compared to a radial flux machine and axial flux machine is in the decoupling of the space requirement of the stator teeth and the armature conductors. As a result, the magnetic and electrical loading can be set independently, which allows for higher torque densities [4]. A TFM suffers from a low power factor and construction complexities [5].

TFMs are generally divided into two broad categories based on their magnet position: surface mounted and flux concentrated. The machines in [6]–[11] are examples of surface-mounted TFMs. The structure generally has U-core stators wherein the alternate poles are not utilized, resulting in a magnet utilization of 50%. The leakage reactance is also high in this topology of motor. An exterior stator version of this motor was presented in [7]. The use of iron bridges in the stator to increase magnet usage was proposed in [8]. The authors in [6] further studied this model and compared it to the traditional TFM through three-dimensional finite element analysis (FEA). According to their analyses, TFMs with iron bridges are superior because they increase the magnet utilization by 84%. A different topology with laminated U-core stators and stator bridges, ring windings, and axially magnetized permanent magnet rings was proposed in [9]. Single-sided TFMs with stator bridges and outer rotors were discussed in [10], [11]. The machine used ring windings and laminated U-shaped stator cores for easier manufacturing.

Another interesting type of TFM is the Z-TFM, discussed in [12]. In the Z-TFM, surface permanent magnets and alternate intermediate poles are used to maximize magnet usage. The output of the machine is twice that of a conventional surface-mounted TFM; however, flux leakage and iron losses are much higher in this machine topology.

A flux-concentrating TFM is the other widely used type of TFM. This type of machine is preferred due to their higher power factor, air gap flux density, and high torque density; however, this type of machine poses a greater challenge in terms of construction. Weh proposed the first double-sided flux-concentrating TFM in [13], [14]. The advantages and disadvantages of different topologies of TFMs were discussed in [16]. The comparison in [15] demonstrated that the surface magnet single sided TFM has a higher torque per volume and torque per mass than the induction machine.

Low power factor is one of the major drawbacks of TFMs [17], [18]. The analysis and comparison in [18] noted that higher ratio of electrical loading to magnetic loading resulted in lowering the power factor. It is also concluded that the flux-concentrating type is superior in terms of power factor due to higher magnetic loading.

A double-sided modular TFM with toroidal windings was proposed in [19]. The winding was exposed to the air in between each stator pole, which helped to improve the cooling of the machine. In this structure, flux-concentrating inset rotor magnets are used with toroidal ring windings. The design allowed for the use of low-remnant flux density permanent magnets. The specific sizing and power density equations related to TFMs are presented in [20].

A machine combining the concept of intermediate poles in [12] and modular toroidal windings with flux-concentrated magnets [19] was presented in [21], [22]. In [21], the authors presented an analytical model of the double-sided flux-concentrating TFM. A machine designed and optimized for in-wheel applications was presented in [22].

This paper presents a systematic approach to the design considerations for the double-sided modular TFM. Initial sizing, pole number selection, and pole shaping are discussed in detail. The effect of pole number with respect to magnetic and electrical loading on the machine's torque density, losses, and power factor are presented. The effect of pole pitch on back-emf, cogging torque, and inductance are also analyzed. The study is carried out with a 48-V, 1.2-kW, 400-rpm, single-phase, direct-drive wind generator as the base design.

II. Direct-Drive Wind Turbine

Wind generator systems are slowly moving away from geared single-speed drives to a direct-drive configuration that increases the system efficiency by avoiding the mechanical losses in the gears [23]. It also increases the system reliability by reducing failures in the gearbox and lowering maintenance downtime. A direct-drive system requires a low-speed, high-torque machine and a power electronic converter for grid connection. Direct-drive generators with permanent magnet excitation offer an added advantage of eliminating excitation losses and reducing the active weight of the machine. The power generation equation for a wind turbine is given in (1):

$$P = \frac{1}{2}\rho\pi R^2 V^3 C_p \tag{1}$$

$$\omega_m = \lambda\frac{V}{R} \tag{2}$$

where ρ is the air density, R is the radius of the turbine blade, V is the wind velocity, C_p is the aerodynamic conversion factor, λ is the tip-speed ratio, and ω_m is the generator speed obtained from (2). Typically, the optimum λ is between 6 and 8, and the optimum C_p is 0.45 [24]. The design parameters, which affect the generator speed, are dependent on the power of the wind turbine. This is illustrated in Fig. 1 and Fig. 2, which show that as the rating of the turbine increases, the speed decreases. C_p and λ were chosen to be fixed at 0.45 and 7, respectively; thus, machines with high torque at low speeds are ideal for wind generator applications. This operating range of low speed and high torque is ideal for transverse flux machines. A 1-kW turbine with a generator speed of 400 rpm is selected as the case study application. The specifications are shown in Table 1.

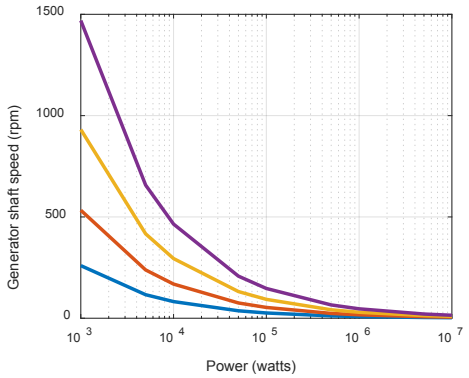

Fig. 1. Shaft speed of turbine for different power ratings and wind speed.

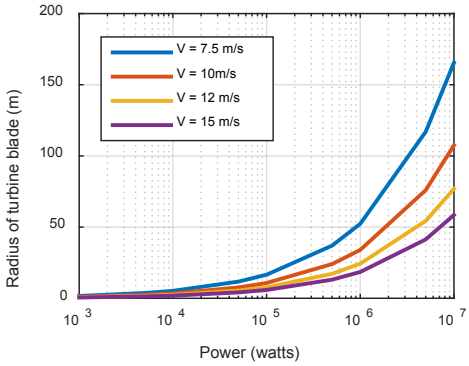

Fig. 2. Rotor radius of turbine for different power ratings and wind speed.

TABLE I. Specification of Case Study Wind Turbine

Axis	Vertical
No. of blades	5
Rotor radius	1.05 m
Cut-in speed	3.4 m/s
Rated wind speed	11 m/s
Rated rotor speed	400 rpm
Rated power	1 kW

III. Design Considerations

The structure of the transverse flux machine investigated in this paper is shown in Fig. 3. The air gap flux is axial, the current is circumferential, and the stator core is oriented in the transverse plane. The magnets in this machine are arranged to concentrate the flux in the air gap, as shown in Fig 4. This magnet arrangement facilitates the use of the cost-effective ferrite magnets while maintaining a high air gap flux density. Because the TFMs suffer from high leakages, magnets with orthogonal magnetization are added between the poles to reduce the leakage flux [22]. The rotor structure and the magnet orientations are shown in Fig 5.

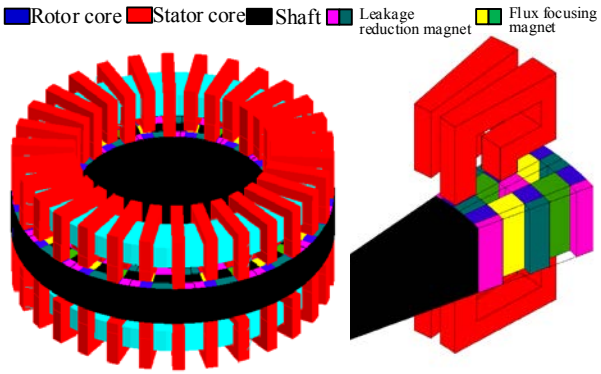

a) Full machine b) One pole pair

Fig. 3. Structure of double-sided flux-concentrating TFM.

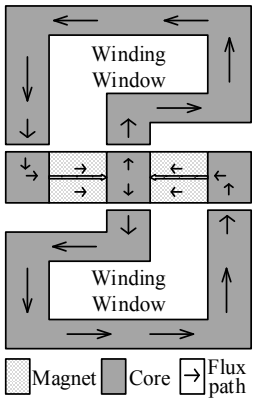

Fig. 4. Flux path in the TFM.

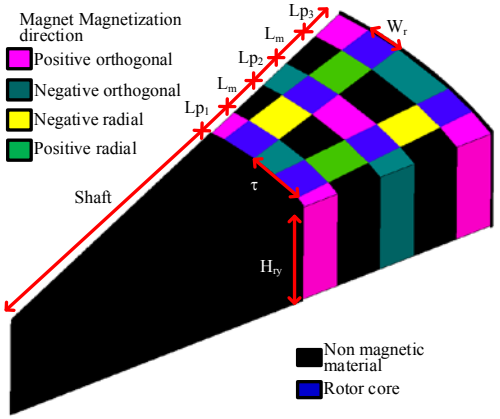

Fig. 5. Parametric description of one rotor pole pair and magnetization direction.

In this machine, quasi-U-shaped stator cores (Fig. 6) are used on two sides of the rotor. A ring winding is employed. This winding arrangement allows the pole numbers to be increased without sacrificing the winding area. The stator cores are arranged so that intermediate poles are utilized. The core in one pole carries the flux from the center rotor to the outer rotor, and the other stator in the intermediate pole carries the flux from the center rotor to the inner rotor. These are alternately arranged on both the upper and lower sides.

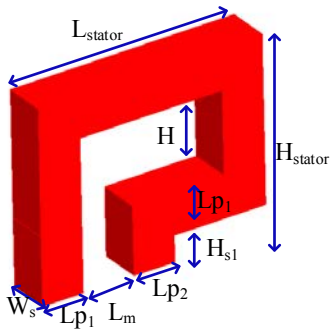

Fig. 6. Parametric description of one quasi-U stator core.

The machines is parametrized quantities their description is given in Table II.

Table II. GEOMETRIC PARAMETERS OF TFM

Shaft	Non-magnetic shaft length	H_{stator}	Height of stator
Lp_1	Inner rotor core length	H_{s1}	Stator clearance height
Lp_2	Center rotor core length	H	Winding window height
Lp_3	Outer rotor core length	W_r	Rotor pole width
L_m	Magnet length	W_s	Stator pole width
L_{stator}	Length of stator	τ	Pole pitch
H_{ry}	Rotor height	$_G$	Air gap length

A. Initial Sizing

The sizing equation for a single-phase TFM can be given by (3):

$$P_o = \eta K_p E_{max} I_{max} \tag{3}$$

$$K_p = \frac{1}{T}\int_0^T \frac{e(t)i(t)}{E_{max}I_{max}}dt \tag{4}$$

where E_{max} and I_{max} are the peak armature winding back-emf voltage and current and K_p is the back-emf waveform factor given in (4). The electromotive force, E, can be expressed as shown in (5):

$$E = NK_e\phi f \tag{5}$$

$$\phi = (1 - P_{embrace})PB_g\pi D_g H_{ry} \tag{6}$$

where N is the number of turns; K_e is the emf factor incorporating the winding distribution factor K and the ratio between the area spanned by the salient poles and the total air gap area; ϕ is the air gap flux; T is the electrical time period; and f is the frequency of the motor, which is dependent on the motor poles and rotational speed. The air gap flux, ϕ, can be obtained from (6), where B_g is the air gap flux density, D_g is the mid-diameter of the air gap, H_{ry} is the rotor core height, and $P_{embrace}$ is the fraction of the pole pitch.

Based on the parametric description of the machine, the D_g and $P_{embrace}$ can be defined as:

$$D_g = shaft + Lp_1 + L_m + 0.5Lp_2 \tag{7}$$

$$P_{embrace} = \frac{W_r}{\tau} \tag{8}$$

These sizing equations can be used to guide the designer when selecting the parameters for an initial design.

B. Pole Number Selection

The homopolar flux path in the stator cores allows for an increase in VA rating of the machine by increasing the pole number for a given machine geometry (outer diameter and axial length), current, and magnetic loading. This can be illustrated by the equation for electrical loading (A_m) (9):

$$A_m = p\frac{\sqrt{2}I_{rms}N}{\pi D_g} \quad (9)$$

In single phase TFMs the number of stator and rotor poles are the same. Increasing the pole number reduces the peripheral length of the poles. The amount of flux linking the stator conductor remains the same (neglecting leakage flux), but the rate of change of flux linkage increases, thereby increasing the back-emf of the machine for the same mechanical speed; however, increasing the pole number increases the flux leakage, which degrades the power factor, thus setting a limit on the number of poles [4]. This is shown in Fig. 7(a).

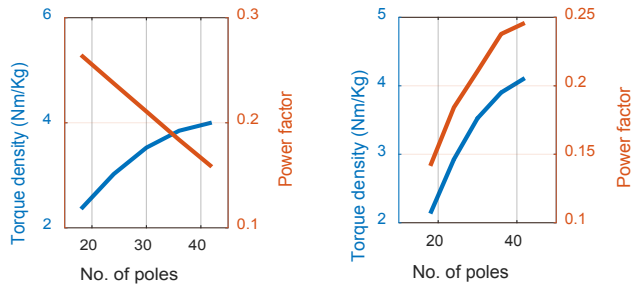

(a) Constant rms current (I_{rms}) for all designs.

(b) Constant electrical load (A_m) for all designs.

Fig. 7. Effect of changing pole numbers on power factor and torque density.

It is possible to maintain the same electrical loading by reducing the current and increasing the pole numbers. This would also result in increasing the torque density by reducing the stator mass. The effect of changing the pole numbers on torque density and power factor with the same current loading is investigated, and the results are shown in Fig. 7(b). Increasing the pole numbers also increases the amount of core losses that affect the motor efficiency, as shown in Fig. 8. The core losses are increased due to the higher excitation frequency at rated speed. In the machine with a fixed current, the efficiency drops after a peak because the core loss dominates; however, in the machine with a fixed A_m, the copper losses are also reduced with increased pole numbers. Copper losses are the dominant loss factor in the investigated range of pole numbers; therefore, a reduction in copper losses results in an overall efficiency increase even if the core losses are increasing.

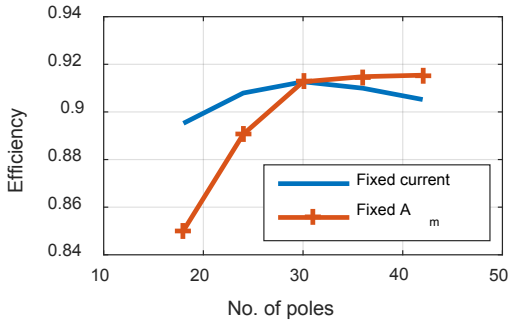

Fig. 8. Effect of changing pole numbers on efficiency.

C. Effect of Key Design Parameters

Key design parameters and design ratios that affect the machine's torque density and power factor are investigated for different pole numbers (18, 30, and 42).

Air gap length l_g: Decreasing the air gap length increases the average torque of the machine by increasing the back-emf voltage, as shown in Fig. 9(a). The machine weight is not affected, thus torque density increases, as shown in Fig. 9(b). Power factor improves with the small air gap due to lower leakage, as shown in Fig. 9(c); however, increased cogging torque and issues with eccentricity limit the air gap length.

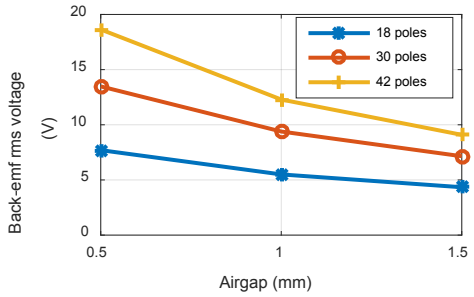

(a) Back-emf rms voltage

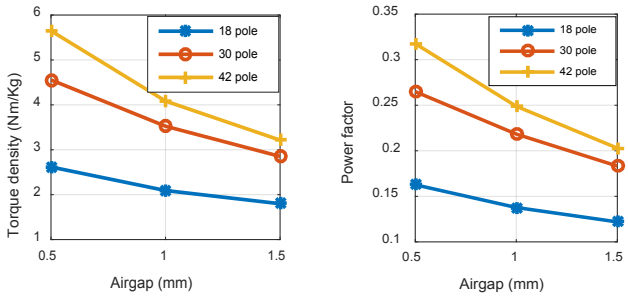

(b) Torque density

(c) Power factor

Fig. 9. Effect of changing air gap with same electric loading and magnet/pole dimensions.

Flux Focusing Factor k_f: The magnetic loading of the machine can be changed by changing the air gap flux density. The focusing factor, k_f, is determined by the ratio

of the magnet face area and the pole face area, as shown in (10):

$$K_f = \frac{B_g}{B_m} = \frac{A_m}{A_p} \tag{10}$$

where B_g is the air gap flux density, B_m is the magnet residual flux density, A_m is the area of the magnet area in the magnetization direction, and A_p is the area of the centre pole in the axial face. Based on the machine's geometric description, the focusing factor can be expressed as:

$$K_f = \frac{W_r Lp_1}{W_r H_{ry}} = \frac{Lp_1}{H_{ry}} \tag{11}$$

The effect of changing the flux-focusing factor on the air gap flux density is shown in Fig. 10.

Increasing the k_f also increases the active weight of the machine; however, the increase in machine torque is more significant, resulting in increased torque density. This effect is more prominent in machines that have high pole numbers, as shown in Fig. 11. Increased magnetic loading also improves the power factor of the machine, as shown in Fig 9. In all of these cases, the electrical loading defined by (9) was kept the same.

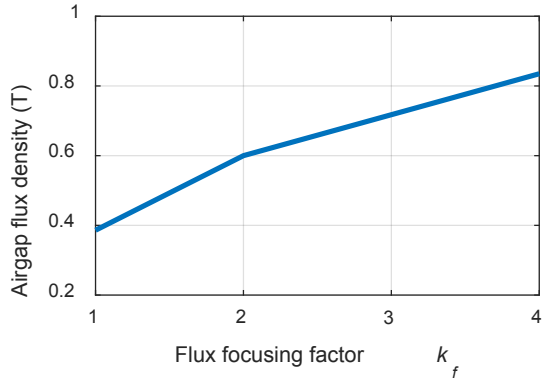

Fig. 10. Effect of k_f on air gap flux density.

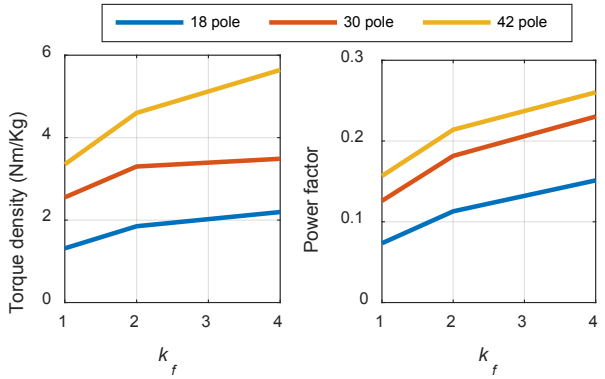

Fig. 11. Effect of k_f on torque density and power factor.

Design ratios λ_D and k_m: To aid the design procedure, a design ratio λ_D is introduced. It is defined as:

$$\lambda_D = \frac{Di}{Do} = \frac{shaft}{shaft + Lp_1 + Lp_2 + Lp_3 + 2L_m} \tag{12}$$

where Di is the inner diameter of the machine, and Do is the outer diameter of the machine. This is a popular design ratio in axial flux machines. The selection of this ratio is a key design step in the design of this topology of machines.

In this machine, laminations are stacked together to form the rotors and stators. As a result, to maintain the same flux in the three rotor poles, the pole lengths are selected to be the same, as expressed by:

$$Lp_1 = Lp_2 = Lp_3 = Lp \tag{13}$$

The investigation for this was carried out by keeping the outer diameter fixed. The width of the pole length and magnet length were changed to vary the inner diameter. For a more convenient analysis, a design ratio k_m is introduced. It is defined as:

$$k_m = \frac{L_M}{Lp} \tag{14}$$

The effect of changing k_m for different λ_D on torque density and power factor is presented in Fig. 12–Fig. 14 for machines with different number of poles. Increasing the λ_D results in a decreasing trend in the power factor and torque density. The results indicate a very nonlinear relationship between k_m and λ_D; thus, a thorough optimization of these parameters is needed. A particle swarm based optimization was carried out for an optimum design. In this research, a 30-pole machine was selected for fabricating (taking cost and construction complexity into account), and it is found that the optimum λ_D for this pole number is at 0.6 for maximum torque density and power factor.

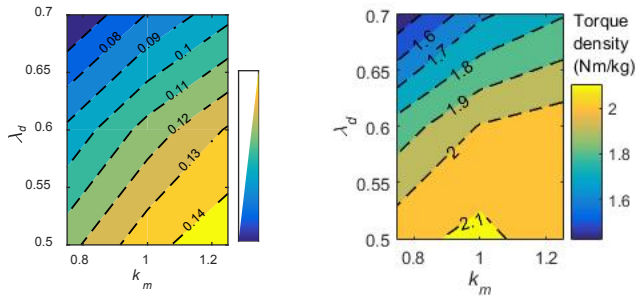

(a) Effect on power factor (b) Effect on torque density

Fig. 12. Effect of λ_D and k_M in an 18-pole machine.

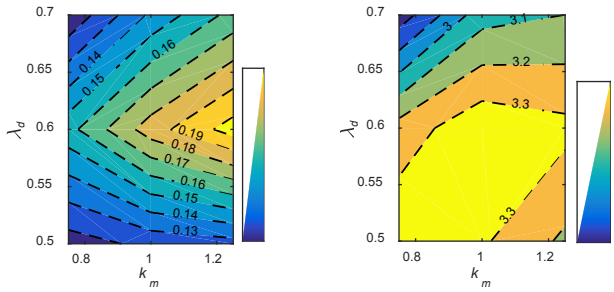

(a) Effect on power factor (b) Effect on torque density

Fig. 13. Effect of λ_D and k_M in a 30-pole machine.

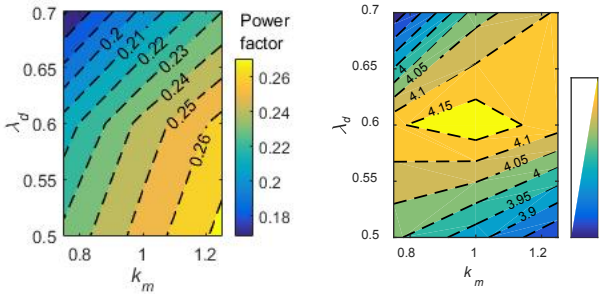

(a) Effect on power factor (b) Effect on torque density

Fig. 14. Effect of λ_D and k_M in a 42-pole machine.

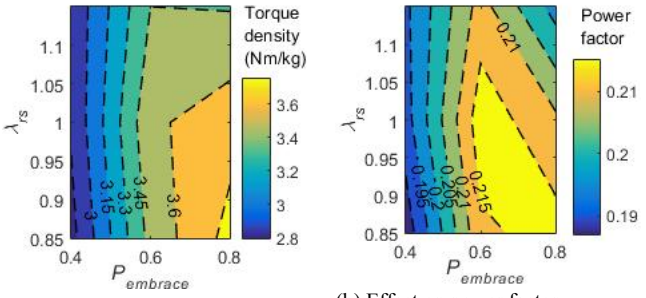

(a) Effect on torque density (b) Effect on power factor

Fig. 15. Effect of $P_{embrace}$ and $\lambda_{r/s}$ on torque density in a 30-pole machine.

D. Pole Pitch

The back-emf waveform is an important design aspect in permanent magnet machines. The permanent magnets in the proposed TFM provides electromechanical coupling between the stator and the rotor; thus, the waveform shape is crucial in the torque production mechanism of permanent magnet machines. The back-emf waveform factor is defined by K_p in (4). The factor in radial machines is shown in (15):

$$K_p = f(L_m, K_d, K_{sl}, K_\alpha K_w) \tag{15}$$

where L_m is the magnet width; and K_d, K_{sl}, K_α and K_w are the distribution, slot, skew, and winding factors, respectively. In radial machines, the winding configuration and stator slot selection play a major role in the back-emf waveform factor.

In the proposed TFM, the rotor and stator pole numbers are the same, and ring windings are used; thus, the waveform factor for the proposed machine would take the form of (16):

$$K_p = f(W_r, W_s, N) \tag{16}$$

$$\lambda_{r/s} = \frac{W_r}{W_s} \tag{17}$$

where W_r and W_s represent the rotor and stator pole widths, respectively. To observe the effect of W_r and W_s, the concept of pole embrace, $P_{embrace}$, is introduced in (8). τ is the pole pitch. The stator pole-to-rotor pole overlap ratio, $\lambda_{r/s}$, is introduced in (17). The effect of changing $P_{embrace}$ and $\lambda_{r/s}$ on torque density and power factor is shown in Fig. 15. It can be observed that as the $P_{embrace}$ is increased, torque density and power factor improve, but with increasing $\lambda_{r/s}$, the torque density and power factor deteriorate.

The back-emf waveform shape becomes more sinusoidal (k_p is decreasing) with increasing $P_{embrace}$ for a fixed $\lambda_{r/s}$, as shown in Fig. 16. The back-emf waveform also becomes more sinusoidal (k_p is decreasing) with a higher ratio of $\lambda_{r/s}$, as shown in Fig. 17.

The effect of the pole pitch on both the inductance when stator and rotor are aligned and unaligned is illustrated in Fig. 18. If the pole embrace is too little, the aligned inductance decreases as expected. Pole embrace beyond an optimum point results in greater leakage. This results in lowering the overall aligned phase inductance. This phenomenon is further supported by the plot of unaligned inductance. The higher pole-to-pole leakage at the high pole embrace results in increasing unaligned inductance. A high $\lambda_{r/s}$ results in lowering the fringing fluxes. As a result, a higher inductance is observed.

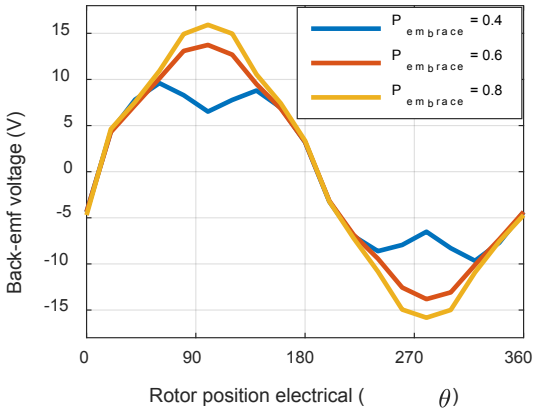

Fig. 16. Effect of $P_{embrace}$ on back-emf wave shape for a 30-pole machine with $\lambda_{r/s} = 1$.

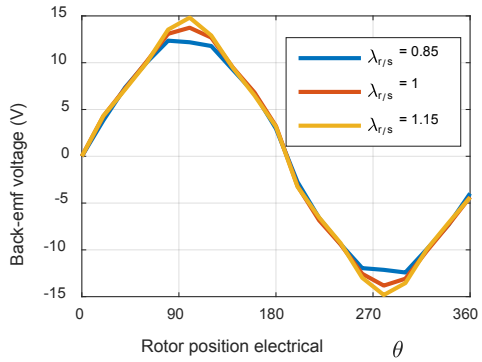

Fig. 17. Effect of $P_{embrace}$ on back-emf wave shape for a 30-pole machine with $\lambda_{r/s} = 1$.

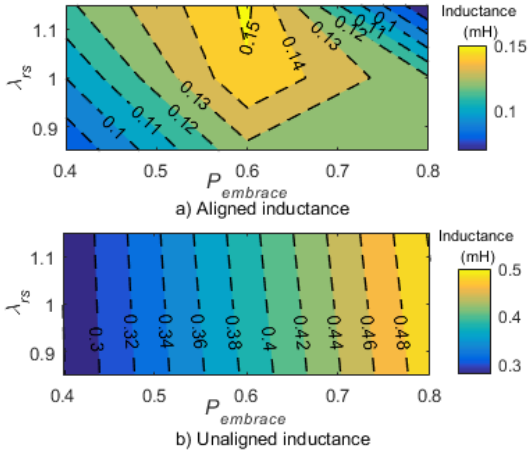

Fig. 18. Effect of $P_{embrace}$ and $\lambda_{r/s}$ on inductance in a 30-pole machine.

E. Material Consideration

The material used for the construction of the machine heavily influences the choice of some of the machine parameters. In the case study application, the rated operating speed is 400 rpm. The choice of the number of poles is dependent on this speed. If a high pole number is selected, the operating frequency would be high. The lamination material and thickness places a limit on the pole number. A lamination steel with a thin gauge would allow for higher pole numbers. In this case study, a 29-gauge M19 steel is selected as the lamination steel. The highest acceptable operating frequency was 100 Hz; thus, a 30-pole machine was selected. A lamination steel with better core-loss properties and/or thinner laminations would have facilitated the use of higher pole numbers for this rated speed. Another option for operating at high frequencies is the use of soft magnetic composite materials for the core [25], [26].

In the case study machine, ferrite magnets are used due to their lower cost. From the preceding sections, it is clear that increasing magnetic loading improves the torque density and power factor of the machine; thus, magnets with higher remanence flux densities such as NdFeB or SmCo would greatly improve the machine's power factor and torque density. A 30-pole machine's performance with different magnets is shown in Table III.

Table III. DESIGN AND PERFORMANCE SPECIFICATIONS

Description	Design I	Design II	Design III
Magnetic material	Ferrite	NdFeB	SmCo
Residual flux density	0.4 T	1.1 T	1.1 T
Relative permeability	1.04	1.05	1.38
Rated speed	400 rpm	400 rpm	400 rpm
Average torque	28.6 Nm	64.5 Nm	60.2 Nm
Output power	225 mm	225 Nm	
Torque density	3.3 Nm/kg	7 Nm/kg	6.2 Nm/kg
Power factor	0.202	0.49	0.45

IV. THREE-DIMENSIONAL FEA ANALYSIS OF FINAL DESIGN

Based on these trends and design considerations, a 30-pole, 400-rpm, 1.2-kW machine has been designed. The electromagnetic analysis was performed in flux 3D. The model was meshed with second-order elements. The mesh of the model is shown in Fig. 19. The machine was designed for a maximum flux density below 2 T, as demonstrated by the flux density at the aligned and unaligned positions in Fig. 20 and Fig. 21. The flux direction during the aligned position is shown in Fig. 22 matches with the hypothesis presented in Fig. 4.

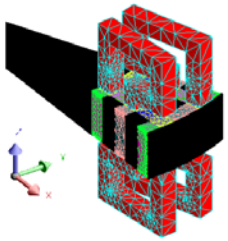

Fig. 19. FEA model with mesh.

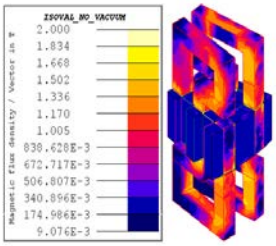

Fig. 20. Flux density at completely aligned position.

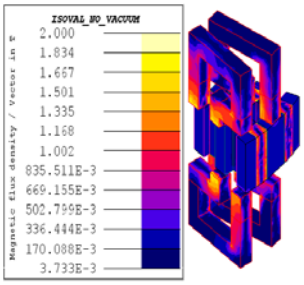

Fig. 21. Flux density at fully unaligned position.

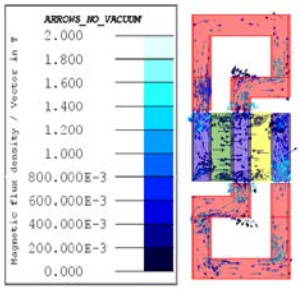

Fig. 22. Flux arrows of magnetic flux at aligned position.

The air gap flux density at the middle of the central rotor core for an entire electrical cycle is shown in Fig. 23. The machine back-emf voltage at 400 rpm for one side is shown in Fig. 24.

The torque and current waveforms for the final design are shown in Fig. 25. A considerable ripple in the torque is observed; however, this is for only one stack of the TFM. Generally, multiple stacks are connected on a single shaft to form a multiphase TFM [10], [11]. A stacked multiphase version of this machine is ideal for real-world applications. Key parameters are shown in Table IV.

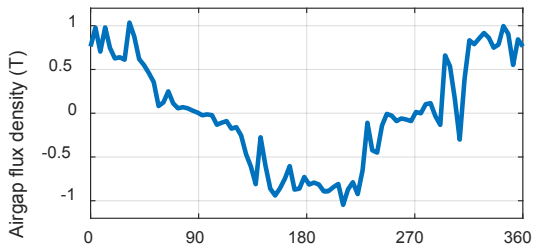

Fig. 23. Air gap flux density at the center point of the rotor for the entire electric cycle.

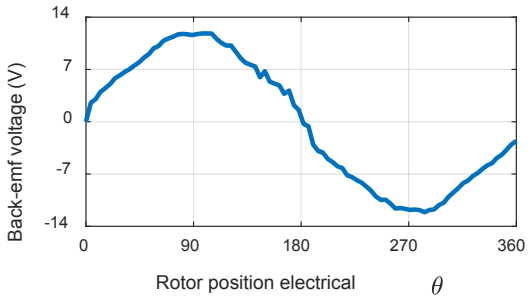

Fig. 24. Back-emf waveform of final design.

Table IV. DESIGN AND PERFORMANCE SPECIFICATIONS

Description	Value	Description	Value
Output power	1.2 kW	Rotor Height	26 mm
Rated speed	400 rpm	Stator clearance	5 mm
Current density	5 A/mm^2	Winding height	16 mm
Air gap length	1 mm	Pole number	30
Axial length	102 mm	DC bus	48 V
Outer diameter	225 mm	Frequency	100 Hz
Rotor core length	8 mm	RMS current	107 A
Magnet length	10 mm	Average Torque	28.6 Nm
Shaft length	68.5 mm	Power factor	0.202
Stator pole width	8.25 mm	Weight	8.69 kg
Rotor pole width	8.25 mm	Torque density	3.28 Nm/kg

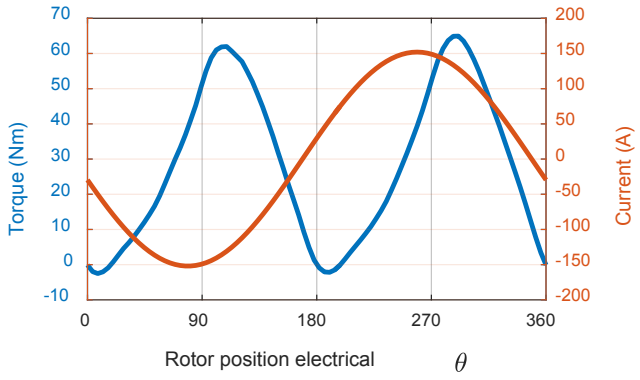

Fig. 25. Torque and current waveform of final design.

V. CONCLUSIONS

This paper presents the design of a modular, single-phase, double-sided TFM with flux-concentrating setup. The flux-concentrating principle allows for the use of low-cost ferrite magnets while maintaining a high air gap flux density. A design procedure was presented for this class of machine and used to design a 1.2-kW machine for direct-drive wind turbine applications. The paper investigated the effects of increasing the number of poles for TFMs on the efficiency, torque density, and power factor. Different design ratios are introduced to facilitate the design process. Their effect on torque density, power factor, and inductance are analyzed. Back-emf shaping through the rotor and stator pole width for different pole pitches have also been presented.

ACKNOWLEDGEMENT

The authors would like to thank the National Science Foundation (NSF Award No. 1307693, 1307846) for funding this research. NREL's contribution to this work was supported by the U.S. Department of Energy under Contract No. DE-AC36-08GO28308 with the National Renewable Energy Laboratory.

REFERENCES

[1] H. Weh and H. May. "Achievable force densities for permanent magnet excited machines in new configurations," in *Proc. 1986 Int. Conf. Electrical Machines,* vol. 3.

[2] H. Weh, "Machine with transverse flux." U.S. Patent No. 5,633,551. 27 May 1997.

[3] H. Weh, H. Hoffmann, and J. Landrath, "New permanent magnet excited synchronous machine with high efficiency at low speeds," in *Proc. 1988 ICEM'88*, Pisa, Italy, pp. 1,107–1,111.

[4] W. M. Arshad, T. Bäckström, and C. Sadarangani, "Analytical design and analysis procedure for a transverse flux machine," in *Proc. 2001 IEEE Conf. Elec. Mach. and Drives*, pp. 115–121.

[5] L. Strete, L. Tutelea, I. Boldea, C. Martis, and I. Viorel, "Optimal design of a rotating transverse flux motor (TFM) with permanent magnets in rotor," in *Proc. 2010 Int. Conf. on Electrical Machines (ICEM)*, Sept..

[6] D. Svechkarenko, J. Soulard, and C. Sadarangani, "Parametric study of a transverse flux wind generator at no-load using three-dimensional finite element analysis," in *Proc. 2009 Int. Conf. Electr. Mach. Syst.*, pp. 1–6.

[7] M. R. Harris, G. H. Pajooman, and S. M. Abu Sharkh, "Performance and design optimisation of electric motors with heteropolar surface magnets and homopolar windings," in *Proc. 1996 IEE Electr. Power Appl.* vol. 143, pp. 429–436.

[8] G. Henneberger, "Development of a new transverse flux motor," *IEE Colloq. New Topol. Perm. Magn. Mach.*, vol. 1997, pp. 1–1, 1997

[9] G. Kastinger, "Design of a novel transverse flux machine," in *Proc. 2002 ICEM*.

[10] J. F. Gieras, "Performance characteristics of a permanent magnet transverse flux generator," in *Proc. 2005 IEEE Conf. Elec. Mach. and Drives*, pp. 1,293–1,299.

[11] J. F. Gieras, "Transverse flux machine." U.S. Patent No. 7,830,057. 9 Nov. 2010.

[12] W. M. Arshad, T. Backstrom, and C. Sadarangani, "Investigating a transverse flux machine with intermediate poles," in *Proc. 2002 Int. Conf. on Power Electronics, Machines and Drives*, pp. 325–328.

[13] H. Weh, H. Hoffmann, J. Landrath, H. Mosebach, and J. Poschadel, "Directly driven permanent magnet excited synchronous generator for variable speed operation," in *Proc. 1988 European Community Wind Energy Conference*, pp. 566–572.
[14] H. Weh, "Transverse-flux machines in drive and generator application," in *Proc. 1995 IEEE Symposium on Electric Power Engineering (Stockholm Power Tech),* Stockholm, Sweden, vol. Invited speaker' session, pp. 75–80.
[15] M. R. Harris and B.C. Mecrow. "Variable reluctance permanent magnet motors for high specific output," in *Proc. 1993 IET Sixth International Conference on (Conf. Publ. No. 376)*.
[16] M. R. Harris, G. H. Pajooman, S. M. A. Sharkh, and S. M. Abu Sharkh, "Comparison of alternative topologies for VRPM (transverse-flux) electrical machines," in *Proc. 1997 IEE Colloq. New Topol. Perm. Magn. Mach. (Digest No 1997/090)*, no. row 8, p. 2/1,2/7.
[17] M. R. Harris, G. H. Pajooman, and S. M. A. Sharkh, "The problem of power factor in transverse flux motors," no. 444, pp. 386–390, 1997.
[18] Z. Y. Z. Yu and C. J. C. Jianyun, "Power factor analysis of transverse flux permanent machines," *2005 Int. Conf. Electr. Mach. Syst.*, vol. 1, pp. 450–453, 2005.
[19] E. Muljadi, C.P. Butterfield, Y.H. Wan, "Axial-flux modular permanent-magnet generator with a toroidal winding for wind-turbine applications," *IEEE Trans. Ind. Appl.*, vol. 35, no. 4, pp.831,836, Jul/Aug 1999.
[20] S. Huang, J. Luo, and T. A. Lipo, "Evaluation of the transverse flux circumferential current machine by the use of sizing equations," in *Proc. 1997 IEEE Conf. Elec. Mach. and Drives,* pp. WB2/15.1-WB2/15.3.
[21] I. Hasan, T. Husain, M. W. Uddin, Y. Sozer, I. Husain, and E. Muljadi, "Analytical modeling of a novel transverse flux machine for direct drive wind turbine applications," in *Proc. 2015 IEEE Energy Conversion Congress and Exposition (ECCE),* pp. 2,161–2,168.
[22] Z. Wan, A. Ahmed, I. Husain, and E. Muljadi, "A novel transverse flux machine for vehicle traction applications," in *Proc. 2015 IEEE Power and Energy Society General Meeting*, Denver, Colorado, July 26–30.
[23] R. Kruse, G. Pfaff, and C. Pfeiffer, "Transverse flux reluctance motor for direct servo drive applications," in *Proc. 1998 IEEE Industry Applications Conference,* vol. 1, pp. 655–662.
[24] H. Li and Z. Chen, "Optimal direct-drive permanent magnet wind generator systems for different rated wind speeds," in *Proc. 2007 Power Electron. Appl. Eur. Conf.*, pp. 1–10.
[25] J. G. Zhu, Y. G. Guo, Z. W. Lin, Y. J. Li, and Y. K. Huang, "Development of PM transverse flux motors with soft magnetic composite cores," *IEEE Trans. Magn.*, vol. 47, no. 2, pp. 4,376–4,383, 2011.
[26] Y. Guo, J. G. Zhu, P. a Watterson, and W. Wu, "Comparative study of 3-D flux electrical machines with soft magnetic composite cores," *IEEE Trans. Ind. Appl.*, vol. 39, no. 6, pp. 1,696–1,703, 2003.